Molecular alignment and orientation with a hybrid Raman scattering technique

Philip J. Bustard, R. Lausten, and Benjamin J. Sussman*
National Research Council of Canada, 100 Sussex Drive, Ottawa, Ontario, Canada K1A 0R6
(Received 17 July 2012; published 26 November 2012)

We demonstrate a scheme for the preparation of molecular alignment and angular momentum orientation using a hybrid combination of two limits of Raman scattering. First a weak, impulsive pump pulse initializes the system via the nonresonant dynamic Stark effect. Then, having overcome the influence of the vacuum fluctuations, an amplification pulse selectively enhances the initial coherences by transient stimulated Raman scattering, generating alignment and angular momentum orientation of molecular hydrogen. The amplitude and phase of the resulting coherent dynamics are experimentally probed, indicating an amplification factor of 4.5. An analytic theory is developed to model the dynamics.

DOI: 10.1103/PhysRevA.86.053419 PACS number(s): 32.80.Qk, 42.65.Dr, 42.50.Hz

I. INTRODUCTION

The preparation of aligned and oriented molecules has been a long-standing goal of quantum control efforts. Early approaches were motivated by the sensitivity of chemical dynamics to the alignment and orientation of reactant molecules [1]. As control techniques have advanced, they have become tools for the preparation of states in subsequent experiments, including high-order harmonic generation [2] and time-resolved molecular dynamics studies [3]. With the development of next-generation light sources, the ability to connect the molecular frame with the laboratory frame has become increasingly important because the ability to determine the structure of single biomolecules would represent a major breakthrough [4,5]. Molecular alignment is typically achieved by application of dynamic Stark control (DSC) using pulsed lasers [6–8]. Orientation has been obtained via hexapole state selection [9], brute-force methods [10,11], and application of alternating and direct current electric fields [12–14]. Here we present a hybrid technique, combining aspects of impulsive nonresonant DSC and transient stimulated Raman scattering [15,16], to generate alignment and angular momentum orientation in molecular hydrogen.

The technique proceeds by exciting a molecular rotational coherence via impulsive DSC using an ultrashort pump pulse. An amplification pulse from a second, phase-independent source is then used to increase the coherence by transient stimulated Raman scattering (SRS). In the absence of the pump, the stimulated scattering would be initialized by the vacuum fluctuations and the molecular dynamics would not be phase stable. With the pump, the amplified coherence is phase stable with respect to the femtosecond-pulse source. The role of the amplification field is similar to that in optical parametric amplification [17] where an amplification field ω_{amp} is used to amplify a lower-frequency signal field ω_{sig} by difference-frequency generation, with the remaining energy transferred to the idler field: $\omega_{\mathrm{id}} = \omega_{\mathrm{amp}} - \omega_{\mathrm{sig}}$. Here, the role of the signal field is replaced by the nonpropagating molecular coherence generated by the pump, which initiates Raman scattering by mixing with the amplifying field. Energy is transferred from the amplification pulse to the molecules as it propagates, thereby increasing the coherence; the remaining energy is transferred to the Stokes field.

This paper is organized as follows: in Sec. II we describe the experimental setup used for control and amplification of rotational dynamics in hydrogen; the results are presented in Sec. III. In Sec. IV we explain the coherent dynamics produced by the technique using a simple theoretical model; the model is used to calculate the observed dynamics in Sec. V.

II. EXPERIMENT

The generation, amplification, and measurement of coherent molecular dynamics uses three distinct optical pulses applied to the sample in succession. A single femtosecond laser source is used to provide a "pump" pulse and a "probe" pulse so that the two pulses have a well-defined phase relationship on every shot. An additional high-energy, picosecond-duration "amplification" pulse is generated by a second laser. The two lasers are electronically synchronized, with no optical phase stabilization; their relative phases will fluctuate independently from shot to shot.

In the first step of the experiment, the pump pulse is used to excite coherent rotational dynamics in the gas sample by impulsive DSC, i.e., impulsive stimulated Raman scattering [8,18]. For impulsive DSC to occur between two rotational levels spaced by frequency Ω, the pump pulse must have duration $\Delta\tau_1 \lesssim 2\pi/\Omega$. In the frequency domain this means that the pulse has a bandwidth spanning both rotational levels, with frequency pairs satisfying the two-photon Raman resonance condition [18]. The pump pulse leaves a small rotational coherence in the gas. In the second step, a longer amplification pulse satisfying $\Delta\tau_2 \gg 2\pi/\Omega$ propagates through the weakly excited sample, generating a Stokes sideband by parametrically mixing with the coherence. The Stokes sideband continues to grow exponentially by transient stimulated Raman scattering from the amplification pulse, resulting in a significantly enhanced, or amplified, coherence. Throughout this amplification, the rotational dynamics are phase coherent with respect to the femtosecond pump-pulse source. The femtosecond probe pulse is then applied to the sample in the third and final step. Coherent rotational dynamics created by the pump and enhanced by the amplification pulse modulate the refractive index of the molecules, scattering probe radiation

*ben.sussman@nrc.ca

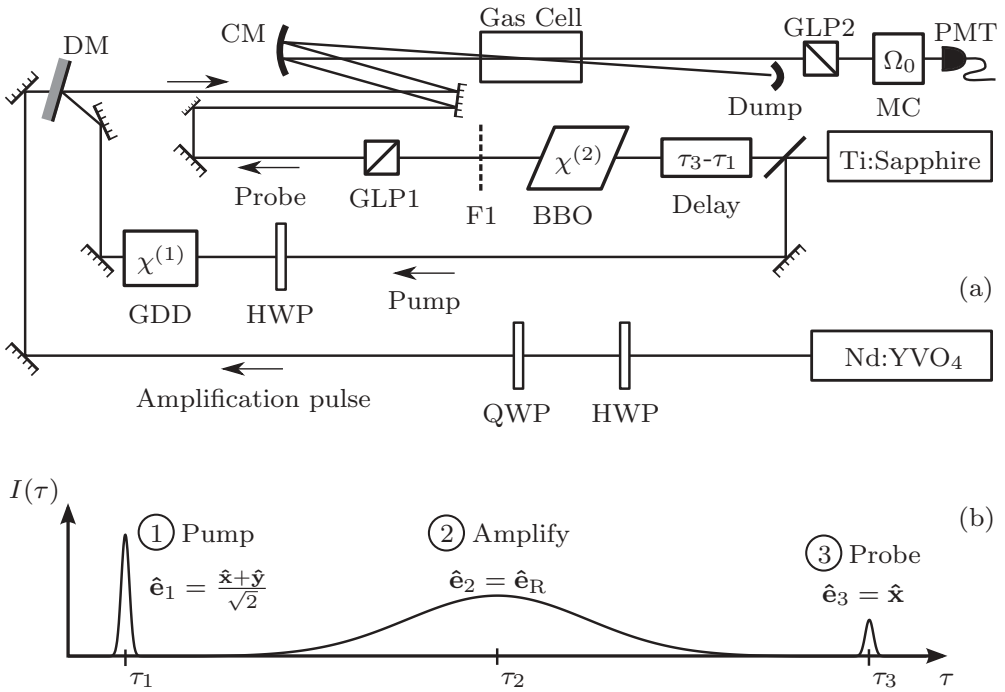

FIG. 1. (a) Diagram of experimental setup. The Ti:sapphire amplifier output is split into a pump path and a probe path. The pump polarization is set at 45° to the horizontal by a half-wave plate (HWP); an SF69 glass block is used to balance the group delay dispersion (GDD). In the probe arm, after a delay stage, the pulse is frequency-doubled using a beta barium borate (BBO) crystal and filtered using BG39 Schott glass (F1); the horizontal ($\hat{\mathbf{x}}$) polarization is cleaned using a Glan-laser polarizer (GLP1). In the amplification beam, pulses from the Nd:YVO_4 amplifier are set to circular polarization using a HWP and quarter-wave plate (QWP). The amplification beam is combined collinearly with the pump beam using a dichroic mirror (DM), and all three beams are brought to focus at the center of a gas cell using a curved mirror (CM). After the cell the probe beam is spatially separated from the pump and amplification beams. A second Glan-laser polarizer (GLP2) is used to reject any remaining $\hat{\mathbf{x}}$-polarized probe light, and the probe is spectrally dispersed using a monochromator (MC) before detection of selected frequencies using a photomultiplier tube (PMT). (b) Time sequence of the pump, amplification, and probe pulses, with peak-intensity times marked on the abscissa.

into Stokes and anti-Stokes sidebands. Detection of the sidebands allows measurement of the rotational dynamics.

A diagram of the experimental setup is shown in Fig. 1(a). A Ti:sapphire amplifier operating at 1 kHz provides pulses of duration 30 fs, centered at $\lambda_1 = 800$ nm; this source is used to generate pump and probe pulses. The amplifier is seeded by an 80-MHz oscillator, locked to an 80-MHz reference clock. A second 80-MHz oscillator, also locked to the reference frequency for pulse synchronization, provides pulses centered at 1.064 μm to seed a Nd:YVO_4 slab amplifier system operating at 1 kHz. The Nd:YVO_4 system outputs 1.6-mJ pulses with duration $\simeq$85 ps, centered at 1.064 μm; these pulses act as the amplification source in the coherence amplification scheme.

The Ti:sapphire output is split into two paths to provide the pump and probe pulses. The first path provides 50-μJ linearly polarized pump pulses polarized at 45° to the horizontal ($\hat{\mathbf{e}}_1$ polarization); an 8-mm block of SF69 glass is included in the path to balance dispersion with the probe beam. In the other path, after a computer-controlled variable delay line, horizontally polarized ($\hat{\mathbf{e}}_3 = \hat{\mathbf{x}}$) probe pulses centered at 400 nm are generated by type I second-order harmonic generation in a 200-μm beta barium borate (BBO) crystal. Residual 800-nm light is filtered from the beam by 3 mm of BG39 glass, and a Glan-laser polarizer is used to maximize the polarization purity of the probe pulses. The circularly polarized ($\hat{\mathbf{e}}_2 = \hat{\mathbf{e}}_R$) amplification beam is combined collinearly with the 800-nm pump beam at a 0° dichroic mirror. The probe beam is aligned parallel to the pump and amplification beams, and all three are brought to a focus in a 7 cm high-pressure gas cell by a curved mirror with focal length $f = 15$ cm. The gas cell is filled with molecular hydrogen at 19 bar. Figure 1(b) shows the time sequence of the pump, amplification, and probe pulse intensities $I(\tau)$, where τ is the time in the pulse frame; the pump, amplification, and probe pulses are centered at τ_1, τ_2, and τ_3, respectively. Figure 2(c) shows an optical cross-correlation in a BBO crystal between the probe and amplification beams; the pump-to-amplification pulse delay time for the experiment was $(\tau_2 - \tau_1) = 100$ ps.

After the cell, the three beams are recollimated at the output of the cell using a focal length $f = 10$ cm lens, and the probe beam is spatially separated from the pump and amplification beams. As in a Kerr cell, a second Glan-laser polarizer with transmission axis in the $\hat{\mathbf{y}}$ direction rejects $\hat{\mathbf{x}}$-polarized probe radiation with a high extinction ratio [19,20]. After the $\hat{\mathbf{y}}$-transmitting polarizer, any remaining probe radiation created by parametric interaction in the cell is dispersed using a Czerny-Turner grating monochromator, and narrow frequency bands from the dispersed probe spectrum are detected using a photomultiplier tube (PMT) whose output is boxcar integrated.

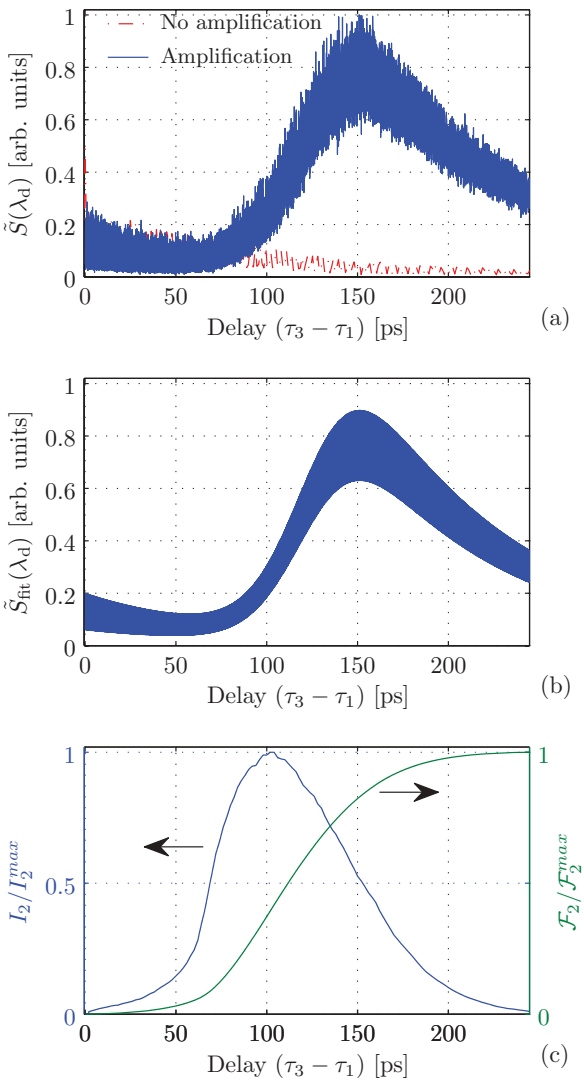

FIG. 2. (Color online) (a) Plot of the integrated PMT signal, detecting the spectral intensity $\tilde{S}(\lambda_d)$ in the probe spectrum at $\lambda_d = 410$ nm as a function probe delay relative to the pump $(\tau_3 - \tau_1)$ with the amplification pulse applied (solid blue line). A low-time-resolution plot shows the effect of dephasing in the absence of the amplification pulse (dash-dotted red line). (b) Theoretical fit of the probe spectral intensity $\tilde{S}_{fit}(\lambda_d)$ as a function of probe delay relative to the pump. (c) Plot of amplification pulse intensity envelope I_2 from cross-correlation with the probe pulse (left ordinate); normalized plot of integrated amplification pulse intensity, or fluence $\mathcal{F}_2$ as a function of probe delay (right ordinate). The spectral intensity in the probe Stokes sideband is a function of the amplification pulse fluence.

III. RESULTS

Figure 2(a) shows a plot (solid blue line) of the measured $\hat{\mathbf{y}}$-polarized probe spectral intensity at $\lambda_d = 410$ nm as a function of pump-probe delay time $(\tau_3 - \tau_1)$; selected high-resolution plots are shown in Figs. 3(a)–3(d). A low-time-resolution scan also plotted in Fig. 2(a) (red dash-dotted line) shows the decaying signal at $\lambda_d = 410$ nm when the amplification pulse is blocked. This wavelength selection is on the Stokes side of the input probe spectrum, at $\delta\bar{\lambda} \approx 587$ cm^{-1} from the center wavelength of the probe, the spectral shift of the purely rotational $S_{00}(1)$ transition in hydrogen [21]. The experimental plot shows creation of coherent rotational dynamics via impulsive DSC by the pump, followed by subsequent amplification of specific rotational coherences by transient stimulated Raman scattering when the amplification pulse is applied. Immediately after the pump, the probe sideband oscillates in amplitude with frequency components at $\nu_1 = 232$ cm^{-1} and $\nu_2 = 227$ cm^{-1}, indicating excitation of coherence between the levels $J \rightarrow J+2$ for $J = 0,1$ (see Sec. V), as is achieved in typical impulsive alignment experiments [20]. The oscillating probe signal subsequently decays during the next ~50 ps due to collisional dephasing of the coherent rotational dynamics [22]. In the absence of an amplification pulse, the signal continues to decay by collisional dephasing. However, as is shown in Fig. 2(a), with the amplification pulse turned on the signal rapidly rises to a peak at 150 ps before again decaying by collisional dephasing when the majority of the amplification pulse energy has passed. The peak signal achieved at $(\tau_3 - \tau_1) = 150$ ps is in excess of that achieved immediately after the pump pulse at short delays, indicating that the amplification pulse amplifies the coherent rotational dynamics excited by the pump. It should be noted that no amplification-pulse dependent signal is observed when the pump beam is blocked, indicating that the amplification pulse energy is not sufficient for any spontaneously initiated stimulated Raman scattering to influence the propagation of the probe pulse. For higher amplification pulse energies, an amplification-pulse dependent signal is expected in the absence of the pump because the Raman excitation can be initiated by spontaneous stimulated Raman scattering. Coherence initiated in this way would not be phase-correlated with the Ti:sapphire probe pulse.

IV. THEORY

A. Model and interaction potentials

We describe the system using a semiclassical model, in which the molecules are treated quantum-mechanically but the optical field is treated as a classical variable. Assuming that we are only concerned with dynamics in the lowest rovibrational levels of the ground electronic state of the molecule, the Hamiltonian for the unperturbed molecular system is

$$\mathcal{H}_{mol} = \sum_j \hbar\Omega_j |j\rangle\langle j|, \tag{1}$$

where $|j\rangle$ are rovibrational states with energy $\hbar\Omega_j$.

We define the qth optical field $\boldsymbol{E}_q(z,\tau) = \frac{1}{2}[\boldsymbol{A}_q(z,\tau)e^{-i\omega_q\tau} + \text{c.c.}]$, where t is the time, z is the propagation coordinate, $\tau = (t - \frac{z}{c})$ is the time in the pulse rest frame assuming no dispersion, ω_q is the carrier frequency of the field, and $\boldsymbol{A}_q(z,\tau)$ is the analytic field. Diffraction is ignored, and so we suppress any dependence on transverse coordinates (x,y). The analytic fields for the pump, amplification, and probe pulses are $\boldsymbol{A}_1(z,\tau)$, $\boldsymbol{A}_2(z,\tau)$, and $\boldsymbol{A}_3(z,\tau)$, respectively; any Stokes sidebands generated by the amplification pulse are labeled $\boldsymbol{B}_{jk}(z,\tau)$, where j labels the lower energy level and k the upper energy level involved in the Stokes transition.

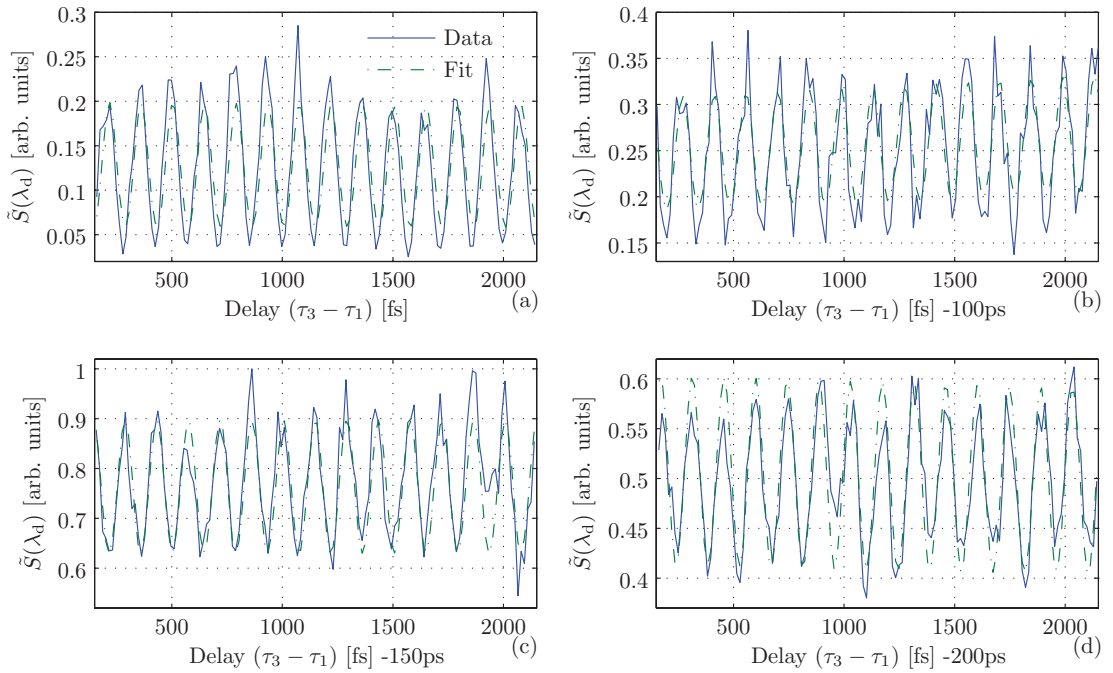

FIG. 3. (Color online) High-resolution extracts from Fig. 2 of measured spectral intensity in the probe spectrum as a function of probe delay. The extracts have start points of (a) $\tau_3 - \tau_1 = 140$ fs, (b) $\tau_3 - \tau_1 = 100.1$ ps, (c) $\tau_3 - \tau_1 = 150.1$ ps, and (d) $\tau_3 - \tau_1 = 200.1$ ps. In each case experimental data (solid blue curve) and a theoretical fit (dashed green curve) are plotted. The fit shows good agreement with the data at all delays.

In the limit where the applied optical fields are far from single-photon resonance with any dipole-allowed transitions to higher energy states, adiabatic elimination of the nonessential upper electronic states gives an effective interaction Hamiltonian $V(z,\tau)$ for Raman transitions within the rovibrational levels [23],

$$V(z,\tau) = -\frac{1}{4}\sum_{qq'} \boldsymbol{A}_q^*(z,\tau)\cdot\boldsymbol{\alpha}\cdot\boldsymbol{A}_{q'}(z,\tau)\mathrm{e}^{-i(\omega_{q'}-\omega_q)\tau}, \quad (2)$$

where $\boldsymbol{\alpha}$ is the molecular polarizability tensor. For the ground-state rotational dynamics considered here, we approximate the polarizability using the static polarizability because the frequency dependence is weak in the visible and near-infrared regions of the spectrum. Equation (2) shows that Raman coupling is proportional to the intensity envelope of the optical field, in contrast to the dipole limit where the dynamics follows the field amplitude.

1. Pump interaction potential

When evaluating the Raman interaction potential of a linearly polarized alignment field, it is usual to choose the $\hat{\mathbf{z}}$ coordinate of the Cartesian coordinates to coincide with the field polarization, resulting in the well-known $\cos^2\theta$ alignment potential [24]. However, since we are later concerned with circularly polarized amplification and Stokes fields, for convenience we set the linearly polarized pump,

$$\boldsymbol{E}_1(z,\tau) = \tfrac{1}{2}[A_1(z,\tau)e^{-i\omega_1\tau} + \text{c.c.}]\hat{\mathbf{e}}_1, \quad (3)$$

where $\hat{\mathbf{e}}_1 = (\hat{\mathbf{x}} + \hat{\mathbf{y}})/\sqrt{2}$. When exposed to such a field, a diatomic molecule like hydrogen, which has polarizability components $\alpha^{xx} = \alpha^{yy} \equiv \alpha_\perp$, and $\alpha^{zz} = \alpha_\parallel$ in the molecular frame (MF), will experience an aligning potential in the laboratory frame (LF) due to the Raman interaction (2). Explicitly evaluating the geometrical dependence of Eq. (2) for Eq. (3) in terms of the Euler angles [25], the interaction potential takes the form

$$V^1(\theta,\phi,z,\tau) = -\frac{1}{4}|A_1|^2\left[\alpha_\perp + \frac{\Delta\alpha}{2}\sin^2\theta\,(1+\sin 2\phi)\right], \quad (4)$$

where $\Delta\alpha = (\alpha_\parallel - \alpha_\perp)$, θ is the polar angle between the molecular axis and the $\hat{\mathbf{z}}$ direction, and ϕ is measured between the $\hat{\mathbf{x}}$ axis and the projection of the molecular axis on the xy plane. For a molecule with $\Delta\alpha > 0$, this potential takes its minimum value for $(\theta = \pi/2, \phi = \pi/4)$ so the molecules tend to align with the field polarization vector $\hat{\mathbf{e}}_1$. The potential is symmetric about the $\phi = \pi/4$ axis.

2. Amplification pulse interaction potential

It can be shown that the gain for rotational stimulated Raman scattering is suppressed for linearly polarized amplification light and takes its maximum value for circularly polarized amplification light, producing opposite circular polarization for the Stokes light [26,27]. As discussed below, the gain for same-circular rotational amplification and Stokes fields is strongly suppressed by Stokes–anti-Stokes (SAS) coupling which inhibits growth of Stokes radiation [16,27]. Amplification of the coherence induced by the pump pulse will therefore be optimized by application of a circularly polarized amplification field. The right-circularly polarized

amplification field is defined as

$$\boldsymbol{E}_2^{\mathrm{R}}(z,\tau) = \tfrac{1}{2}[A_2(z,\tau)e^{-i\omega_2\tau} + \text{c.c.}]\hat{\mathbf{e}}_{\mathrm{R}}. \quad (5)$$

Due to SAS coupling this only drives growth for Stokes radiation with left-circular polarization $\hat{\mathbf{e}}_{\mathrm{L}}$. The Stokes field is defined as

$$\boldsymbol{E}_S^{\mathrm{L}}(z,\tau) = \frac{1}{2}\sum_{j,k>j}\left[B_{jk}^{\mathrm{L}}(z,\tau)e^{-i(\omega_2-\Omega_{kj})\tau} + \text{c.c.}\right]\hat{\mathbf{e}}_{\mathrm{L}}.$$

The interaction potential coupling $\boldsymbol{E}_2^{\mathrm{R}}(z,\tau)$ with $\boldsymbol{E}_S^{\mathrm{L}}(z,\tau)$ is given by

$$\begin{aligned} V^{2\mathrm{R}} &= -\frac{1}{4}\sum_{j,k>j}\left[\left(A_2^* B_{jk}^{\mathrm{L}} e^{i\Omega_{kj}\tau}\right)\hat{\mathbf{e}}_{\mathrm{R}}^*\cdot\boldsymbol{\alpha}\cdot\hat{\mathbf{e}}_{\mathrm{L}} + \text{c.c.}\right] \\ &= -\frac{\Delta\alpha}{8}\sum_{j,k>j}\left(A_2^* B_{jk}^{\mathrm{L}} e^{i\Omega_{kj}\tau}e^{i2\phi}\sin^2\theta + \text{c.c.}\right). \quad (6) \end{aligned}$$

For the alternative case of a left-circularly polarized amplification field and right-circularly polarized Stokes field, the interaction potential is

$$\begin{aligned} V^{2\mathrm{L}} &= -\frac{1}{4}\sum_{j,k>j}\left[\left(A_2^* B_{jk}^{\mathrm{R}} e^{i\Omega_{kj}\tau}\right)\hat{\mathbf{e}}_{\mathrm{L}}^*\cdot\boldsymbol{\alpha}\cdot\hat{\mathbf{e}}_{\mathrm{R}} + \text{c.c.}\right] \\ &= -\frac{\Delta\alpha}{8}\sum_{j,k>j}\left(A_2^* B_{jk}^{\mathrm{R}} e^{i\Omega_{kj}\tau}e^{-i2\phi}\sin^2\theta + \text{c.c.}\right). \quad (7) \end{aligned}$$

Comparison of Eqs. (6) and (7) shows that, unlike Eq. (4), the potentials due to a circular amplification pulse and opposite Stokes are not symmetric with respect to ϕ. Application of a sufficiently powerful circularly polarized amplification field will therefore induce stimulated Raman scattering and break the symmetry about the $\phi = \pi/4$ axis. As a result, $V^{2\mathrm{R}}$ and $V^{2\mathrm{L}}$ are potentials which drive angular momentum orientation of the molecules in the $-\hat{\mathbf{z}}$ or $+\hat{\mathbf{z}}$ direction, respectively. This is in contrast with the impulsive pump potential (4) which drives alignment of the molecules along the pump polarization axis, but with no preferred direction in space.

B. Coherence and selection rules

The coherences contributing to the probe signal can be established by considering the selection rules for the pump, amplification, and probe pulses, with unit polarization vectors $\hat{\mathbf{e}}_1$, $\hat{\mathbf{e}}_2$, and $\hat{\mathbf{e}}_3$, respectively. For convenience when dealing with circular polarizations, we choose the $\hat{\mathbf{z}}$ axis to be the direction of propagation for the three beams, neglecting the small lateral tilt of the probe beam so that all polarization vectors lie in the xy plane. The $\hat{\mathbf{x}}$ axis is selected as the direction of polarization for the probe pulse so $\hat{\mathbf{e}}_3 = \hat{\mathbf{x}}$, with all other polarizations defined relative to these fixed axes in a right-hand coordinate system.

The molecules are modeled in the rigid rotator rotational basis, which is specified in terms of the quantum numbers for the angular momentum J, and its projection M on the LF z axis [21]. The field-free eigenfunctions are spherical harmonics $Y_J^M(\theta,\phi)$, with energy $\hbar\Omega_J = BJ(J+1)$ where B is the rotational constant for the molecule. Each energy level has degeneracy $g_J = (2J+1)$; for each J, M takes integer values $|M| \leqslant J$. For reference, the matrix elements of $e^{\pm i2\phi}\sin^2\theta$ are given in Appendix A.

1. Pump excitation

The pump interaction [see Eqs. (2) and (4)] is governed by selection rules $\Delta J = 0, \pm 2$ and $\Delta M = 0, \pm 2$. The pump pulse will excite coherences with $\Delta J = \pm 2$ provided that it is sufficiently short to satisfy the criterion for impulsive excitation: it must have a duration $\Delta\tau_1 \lesssim 2\pi/(\Omega_{J+2} - \Omega_J)$, where $\hbar\Omega_J$ is the energy of the rotational level with quantum number J.

The pump polarization, at 45° to the horizontal $\hat{\mathbf{x}}$ axis, may be written

$$\begin{aligned} \hat{\mathbf{e}}_1 &= (\hat{\mathbf{x}} + \hat{\mathbf{y}})/\sqrt{2} \\ &= e^{i\pi/4}(\hat{\mathbf{e}}_{\mathrm{R}} - i\hat{\mathbf{e}}_{\mathrm{L}})/\sqrt{2}, \end{aligned} \quad (8)$$

where $\hat{\mathbf{e}}_{\mathrm{R}} = (\hat{\mathbf{x}} - i\hat{\mathbf{y}})/\sqrt{2}$ and $\hat{\mathbf{e}}_{\mathrm{L}} = (\hat{\mathbf{x}} + i\hat{\mathbf{y}})/\sqrt{2}$ are unit vectors for right-circular and left-circular polarizations, respectively. The states coupled by the pump are calculated by evaluating the double product $\hat{\mathbf{e}}_1^*\cdot\boldsymbol{\alpha}\cdot\hat{\mathbf{e}}_1$, which expands to give four terms,

$$\begin{aligned} \hat{\mathbf{e}}_1^*\cdot\boldsymbol{\alpha}\cdot\hat{\mathbf{e}}_1 = \tfrac{1}{2}\big(&\hat{\mathbf{e}}_{\mathrm{R}}^*\cdot\boldsymbol{\alpha}\cdot\hat{\mathbf{e}}_{\mathrm{R}} + \hat{\mathbf{e}}_{\mathrm{L}}^*\cdot\boldsymbol{\alpha}\cdot\hat{\mathbf{e}}_{\mathrm{L}} \\ &+ i\hat{\mathbf{e}}_{\mathrm{L}}^*\cdot\boldsymbol{\alpha}\cdot\hat{\mathbf{e}}_{\mathrm{R}} - i\hat{\mathbf{e}}_{\mathrm{R}}^*\cdot\boldsymbol{\alpha}\cdot\hat{\mathbf{e}}_{\mathrm{L}}\big). \end{aligned} \quad (9)$$

Using the recursion relations for spherical harmonics, the selection rules for Stokes transitions $J \to J+2$ are $\Delta M = \pm 2, 0$. The relevant transitions from Eq. (9) are indicated in Fig. 4.

2. Amplification pulse excitation

The amplification pulse propagates through the sample, amplifying the coherences that were generated by the pump. Which coherences are amplified depends both on the selection rules for the amplification-pulse–Stokes interaction [see Eqs. (2), (6), and (7)] and propagation effects that can suppress growth of specific coherences.

When a right-circularly polarized amplification pulse ($\hat{\mathbf{e}}_{\mathrm{R}}$) propagates through the medium concurrent with $\hat{\mathbf{e}}_{\mathrm{L}}$-polarized Stokes light, the excitation selection rules are $J \to J+2$ and $M \to M-2$ ($\Delta M = -2$). This will be an amplified processes.

When a right-circularly polarized amplification pulse ($\hat{\mathbf{e}}_{\mathrm{R}}$) propagates through the medium concurrent with $\hat{\mathbf{e}}_{\mathrm{R}}$-polarized Stokes light, the excitation selection rules are $J \to J+2$ and $M \to M$ ($\Delta M = 0$). This will be a suppressed processes.

Suppression or amplification of the two processes is due to Stokes–anti-Stokes coupling present in the collinear experimental geometry. Because anti-Stokes generation (from $J+2 \to J$) is also possible (reverse arrows in Fig. 4), there are competing processes. The two specific processes $\Delta J = +2$, $\Delta M = 0$ (Stokes) and $\Delta J = -2, \Delta M = 0$ (anti-Stokes) couple the same states. This balanced coupling for the two processes results in suppressed growth for both: the growth of the Stokes field is inhibited by the loss of the anti-Stokes field [16,27]. As a result, the pumped coherences with $\Delta M = 0$ are not well amplified by the amplification pulse. In contrast, no such competing coupling occurs for the $\Delta M = -2$ Stokes process, which is therefore amplified.

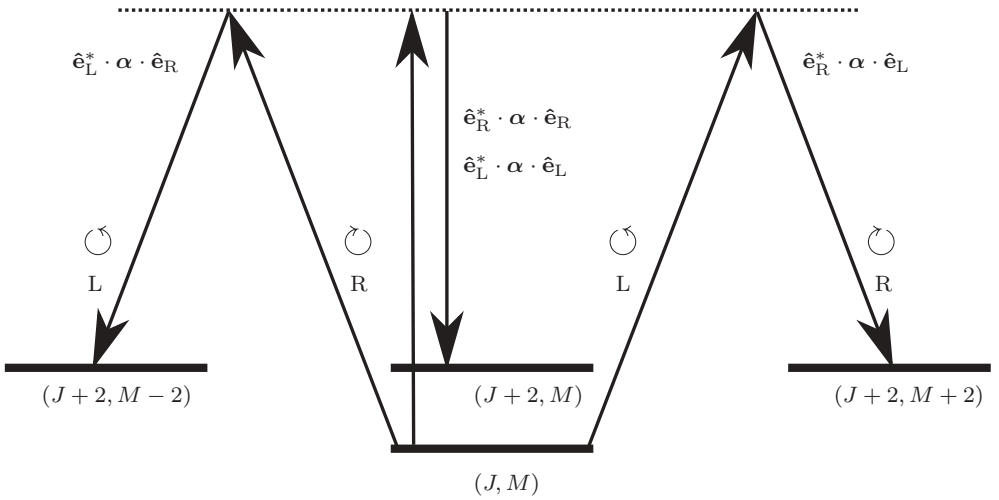

FIG. 4. Energy-level diagram showing the selection rules for Stokes scattering from a lower energy state with rotational quantum numbers (J,M). Right-circularly polarized photons ($\hat{\mathbf{e}}_{\mathrm{R}}$) will scatter to left-circularly polarized Stokes photons ($\hat{\mathbf{e}}_{\mathrm{L}}$), with the system transferring from $(J,M)\rightarrow(J+2,M-2)$. Left-circularly polarized photons ($\hat{\mathbf{e}}_{\mathrm{L}}$) will scatter to right-circularly polarized Stokes photons ($\hat{\mathbf{e}}_{\mathrm{R}}$), with the system transferring from $(J,M)\rightarrow(J+2,M+2)$. In the case of a linearly polarized pump pulse, both types of Stokes transitions will occur for a particular (J,M) state if the pulse is sufficiently short to achieve impulsive DSC. For a circularly polarized amplification pulse, only one set of Stokes transitions, $\Delta M=+2$ or $\Delta M=-2$, will occur, depending on whether the amplification pulse has polarization $\hat{\mathbf{e}}_{\mathrm{L}}$ or $\hat{\mathbf{e}}_{\mathrm{R}}$, respectively. For a linearly polarized probe pulse, both Stokes transitions are possible and will proceed depending on the initial coherence in the system. After coherence enhancement by the amplification pulse with $\hat{\mathbf{e}}_{\mathrm{R}}$ polarization, the probe will Stokes scatter more from the $\Delta M=-2$ transition than from the $\Delta M=+2$ transition. Anti-Stokes scattering of the probe is also observed, with the direction of the arrows reversed in the diagram.

3. Probe scattering

When the probe propagates through a sample excited by the pump and amplification pulses, it drives the electrons with frequency ω_3. The electron motion is modulated by the internal rotational motion with frequencies $(\Omega_{J+2}-\Omega_J)$, resulting in the production of Stokes and anti-Stokes sidebands in the probe spectrum with frequencies $\omega_3-(\Omega_{J+2}-\Omega_J)$ and $\omega_3+(\Omega_{J+2}-\Omega_J)$, respectively.

The PMT detects $\hat{\mathbf{y}}$-polarized radiation scattered from the $\hat{\mathbf{e}}_3=\hat{\mathbf{x}}$ polarized input probe field. In terms of the $(\hat{\mathbf{e}}_{\mathrm{R}},\hat{\mathbf{e}}_{\mathrm{L}})$ basis, the detected field has only a $\hat{\mathbf{y}}$-polarization component,

$$\hat{\mathbf{y}}\cdot\boldsymbol{\alpha}\cdot\hat{\mathbf{e}}_3=\frac{1}{2i}(\hat{\mathbf{e}}_{\mathrm{R}}^{*}\cdot\boldsymbol{\alpha}\cdot\hat{\mathbf{e}}_{\mathrm{L}}-\hat{\mathbf{e}}_{\mathrm{L}}^{*}\cdot\boldsymbol{\alpha}\cdot\hat{\mathbf{e}}_{\mathrm{R}}). \tag{10}$$

Both the $\Delta M=\pm2$ Stokes transitions indicated in Fig. 4 are therefore detected by the PMT, one with $\hat{\mathbf{e}}_{\mathrm{L}}$-polarized Stokes light, and the other with $\hat{\mathbf{e}}_{\mathrm{R}}$-polarized Stokes light. The arrows in Fig. 4 may be reversed, showing the allowed anti-Stokes transitions with $\Delta M=\pm2$. We confirmed the presence of both sidebands in the probe spectrum by observing a similar signal to Fig. 2(a) for the anti-Stokes sideband.

C. Sequential solution

To calculate the signal measured using the photomultiplier, we use a density matrix calculation for the coherent molecular dynamics which are described by Eqs. (4) and (6). This yields coupled equations for the field and material evolution which may be solved in the limit of undepleted amplification and pump pulses [18,28]. The full method of solution is detailed in Appendix B.

1. Pumping by impulsive dynamic Stark control

After propagation of a δ-function pump pulse, $|A_1(\tau)|^2=\mathcal{I}_1\delta(\tau-\tau_1)$ where $\mathcal{I}_1$ is an intensity scaling parameter, the coherence left in the molecules is given by

$$\rho_{jk}(z,\tau>\tau_1)=-i\frac{w_{jk}}{4\hbar}\mathcal{I}_1U_{jk}^{\mathrm{lin}}e^{-\Gamma_{kj}(\tau-\tau_1)}e^{i\Omega_{kj}(\tau-\tau_1)}, \tag{11}$$

where $w_{jk}=(\rho_{jj}-\rho_{kk})$ is the population difference between levels $|j\rangle$ and $|k\rangle$, Γ_{kj} is a phenomenological dephasing constant, and, cf. Eq. (4),

$$U^{\mathrm{lin}}(\theta,\phi)=\left[\alpha_\perp+\frac{\Delta\alpha}{2}\sin^2\theta\,(1+\sin2\phi)\right]$$

contains the angular dependence of the alignment potential. Solution (11) shows that the pump pulses excite coherences which evolve at frequency Ω_{kj}; the amplitude of each coherence scales linearly with the pump-pulse energy.

2. Amplification by transient stimulated Raman scattering

Assuming negligible population transfer during the amplification stage, so w_{jk} is a constant, and negligible depletion of the amplification pulse such that $A_2(z,\tau)=A_2(\tau)$, an analytic solution for the coherence may be found, using Eq. (11) as an initial condition. With the initial Stokes fields $B_{jk}^{\mathrm{L}}(0,\tau)=0$, the amplified coherence is given at times $\tau>\tau_1$ by

$$\rho_{jk}=-i\frac{w_{jk}}{4\hbar}\mathcal{I}_1U_{jk}^{\mathrm{lin}}I_0[\sqrt{4h_{jk}(\tau)z}]e^{-\Gamma_{kj}(\tau-\tau_1)}e^{i\Omega_{kj}(\tau-\tau_1)}, \tag{12}$$

where $I_0(x)$ is the modified Bessel function of order 0,

$$h_{jk}(\tau) = \kappa_{jk}\beta_{kj}\int_{\tau_A}^{\tau} |A_2(\tau')|^2 d\tau', \tag{13}$$

$$\kappa_{jk} = \frac{\Delta\alpha w_{jk}}{8\hbar}\langle e^{i2\phi}\sin^2\theta\rangle_{jk}, \tag{14}$$

$$\beta_{kj} = \frac{(\omega_2 - \Omega_{kj})N\Delta\alpha}{4\epsilon_0 c}\langle e^{-i2\phi}\sin^2\theta\rangle_{kj}, \tag{15}$$

and N is the number density of the sample.

Equation (12) shows that the initial coherence present in the system is amplified by stimulated Raman scattering. Examining the matrix elements of κ_{jk} shows that the only nonzero values occur for $\kappa_{J,M;J+2,M-2}$, and so only these coherences are amplified. The excitation generated by the pump parametrically excites further Raman scattering events when the amplification pulse propagates through the pumped medium. The onset of SRS generates the Stokes field and enhances the molecular coherence. It is worth noting that the phase of the excitation depends only on $(\tau - \tau_1)$, and is independent of the amplification pulse phase. Provided that the ultrashort pump pulse satisfies the limit for impulsive DSC, a phase-independent amplification pulse can be used to enhance the coherence by transient SRS. While the amplified coherences are linearly proportional to the pump intensity, they grow nonlinearly with amplification pulse fluence (integrated intensity) and distance through the interaction region.

3. *Parametric scattering of probe pulse*

The rotational coherence is measured by scattering an ultrashort probe pulse with frequency ω_3 from the excited molecules, and measuring only the $\hat{\mathbf{y}}$-polarized scattered light. Assuming that the molecular coherence is unchanged by the propagation of the probe pulse, Eq. (12) may be used to calculate the medium polarization. For an input field of the form

$$\boldsymbol{E}_3(z,\tau) = \tfrac{1}{2}\left\{\left[A_3^x(z,\tau)\hat{\mathbf{x}} + A_3^y(z,\tau)\hat{\mathbf{y}}\right]e^{-i\omega_3\tau} + \text{c.c.}\right\},$$

where $A_3^y(0,\tau) = 0$, the measured output field at $z = L$ is given by

$$\begin{aligned} A_3^y(z,\tau) = {} & \frac{N\omega_3\Delta\alpha}{8\epsilon_0 c}A_3^x(\tau)\int_0^L dz \\ & \times \sum_{JM}\left\{\left[\rho_{J+2,M-2;JM}\left(H_J^{-M}H_{J+1}^{-M+1}\right)\right.\right. \\ & - \rho_{J+2,M+2;JM}\left(H_J^{M}H_{J+1}^{M+1}\right)\Big] \\ & + \left[\rho_{J,M;J+2,M+2}\left(H_J^{M}H_{J+1}^{M+1}\right)\right. \\ & \left.\left. - \rho_{J,M;J+2,M-2}\left(H_J^{-M}H_{J+1}^{-M+1}\right)\right]\right\}, \end{aligned} \tag{16}$$

and the quantities H_J^M are defined in Appendix A. The first term in square brackets in Eq. (16) generates blueshifted, or anti-Stokes, sidebands, while the second term in square brackets generates redshifted, or Stokes, sidebands in the spectrum. Evaluating the integral over z for the coherences (12) and transforming to the Fourier domain yields a function for the Stokes field, the integrated intensity of which can be fit to the measured data. The pump-pulse fluence, the amplification-pulse fluence, and the initial phase of the molecular coherence are free parameters in the fit.

V. DISCUSSION

A plot of the signal fit $\tilde{S}_{\text{fit}}(\lambda_d) \propto |\tilde{A}_3^y|^2$ in Fig. 2(b), calculated using Eq. (16), shows good functional agreement with the experimental data in Fig. 2(a). The initial coherence, generated by the pump pulse via impulsive DSC, decays exponentially during the first ≈50 ps due to collisional dephasing. The signal then begins to rise rapidly to a peak at 150 ps, before again declining at greater pump-probe delay times due to collisional dephasing. Figure 2(c) shows a plot of the amplification pulse intensity and fluence as a function of time. Comparison of Figs. 2(a) and 2(b) with Fig. 2(c) shows that, as expected, the coherence amplification is a function of amplification pulse fluence rather than intensity. The functional dependence on fluence is a general feature of transient stimulated Raman scattering, in contrast to the steady-state regime where the Stokes intensity is a function of the instantaneous amplification pulse intensity [28]. The coherence amplification technique may therefore be a useful method for preparation of field-free coherent rotational or vibrational motion because the dynamics generated by the amplification pulse will persist after the amplification pulse is turned off, until they are destroyed by collisional dephasing.

Figure 3 shows high-resolution extracts from the experimental and theoretical signals at several probe delays. The measured probe signal shows clear oscillations throughout the measurement, indicating that the coherence is phase stable with respect to the probe pulse at all delays, despite the use of a phase-independent amplification pulse to amplify the coherence. The oscillation frequency is $4B$, where B is the rotational constant for the molecule. The pump and amplification pulses excite coherences between $J \to J+2$, which evolve at $\Omega_{J+2} - \Omega_J = 4B(J+3/2)$. The measured signal has the form

$$\tilde{S}(\lambda_d) \propto \left|\tilde{A}_3^y(z,\lambda_d)\right|^2$$

and contains oscillatory exponential factors with the form $e^{i4B(J-J')(\tau_3-\tau_1)}$. The angular momentum quantum number difference $(J - J')$ takes values $0, \pm 1, \pm 2, \ldots$, so the signal will contain a static background plus oscillations at $4B, 8B, 12B, \ldots$. In the case of hydrogen, level $J = 1$ is most heavily populated (≈66%), with $J = 0$ and $J = 2$ (≈12%) next highest in occupation number, and so the strongest oscillation has frequency $4B$.

Figure 5 shows the coherence amplification ratio $|\rho_{J,M;J+2,M-2}|/|\rho_{J,M;J+2,M-2}(0)|$ as a function of time for molecules at the end of the interaction region in the initial state (J,M). The coherence corresponding to Stokes transitions from $(J = 1, M = -1) \to (3, -3)$ is amplified by a factor of 4.5 at its maximum value while transitions from $(0,0) \to (2, -2)$ and $(1,0) \to (3, -2)$ are both amplified by a factor of ≈2. After full passage of the amplification pulse at 250-ps delay, the $(1, -1) \to (3, -3)$ coherence is still amplified by a factor of ≈3 over its initial value.

It is difficult to make precise measurements of field strengths and mode overlap in the interaction region; however, estimates of the coherence in the sample can be made using Eqs. (B2) and (B5). Using Eq. (B2), a 50-μJ pump pulse is estimated to produce a coherence of $|\rho_{1,-1;3,-3}(0 \leqslant z \leqslant L, 100\text{ fs})| \sim 0.037$. After amplification, at the end of the

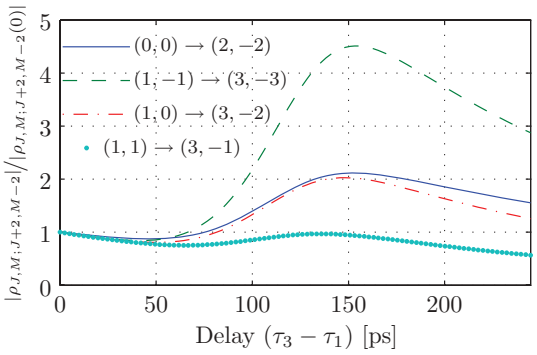

FIG. 5. (Color online) Plot of the coherence amplification ratio $|\rho_{J,M;J+2,M-2}|/|\rho_{J,M;J+2,M-2}(0)|$ as a function of time for molecules at the end of the interaction region. The legend indicates the initial (J,M) state for the Stokes transition $J \to J+2$, $M \to M-2$.

interaction region, the peak coherence is then estimated to be $|\rho_{1,-1;3,-3}(z = L, 150\ \text{ps})| \sim 0.17$ in the present setup. Equation (B5) shows that the amplified coherence grows nonlinearly with the amplification pulse fluence: a small increase in the fluence can produce further increases in the coherence enhancement. Eventually, due to amplification pulse depletion and increased population transfer, Eq. (B5) breaks down so that the dynamical equations (B3) and (B4) must be solved numerically. Numerical evaluation of these equations indicates that off-diagonal coherence of ~0.5 can be approached at the end of the interaction region using larger amplification pulse fluences; similar results have been reported for other Raman-based control schemes [29].

The coherence amplification technique was demonstrated here in hydrogen; however, it may find application in vibrational and rotational control of other molecules, when higher amplification pulse energies are available, thereby enabling Stokes growth. This flexibility is an advantage of the approach because no tuning of the amplification field is required: by generating an initial coherence using the pump pulse, the resulting Stokes sidebands on the amplification pulse are automatically tuned to resonance.

VI. CONCLUSION

In conclusion, we have demonstrated a form of molecular alignment and angular momentum orientation control through selective coherence amplification. The generated molecular rotational coherence is phase stable with respect to an ultrashort pulse source, despite being amplified by transient stimulated Raman scattering using a phase-independent amplification pulse. Angular momentum orientation is achieved by use of a circularly polarized amplification pulse which breaks the symmetry of the alignment potential. By increasing the amplification pulse fluence, the technique has the potential to generate large molecular coherence in control experiments.

ACKNOWLEDGMENTS

We wish to thank I. A. Walmsley for extremely valuable discussions and support. We are grateful to M. Spanner for thoughtful comments on the manuscript.

APPENDIX A: MATRIX ELEMENTS $e^{\pm i2\phi}\sin^2\theta$ FOR DIATOMIC MOLECULES

The matrix elements of $e^{i2\phi}\sin^2\theta$ and $e^{-i2\phi}\sin^2\theta$ arise from the polarization products $\hat{\mathbf{e}}_{\mathrm{R}}^{*}\cdot\boldsymbol{\alpha}\cdot\hat{\mathbf{e}}_{\mathrm{L}}$ and $\hat{\mathbf{e}}_{\mathrm{L}}^{*}\cdot\boldsymbol{\alpha}\cdot\hat{\mathbf{e}}_{\mathrm{R}}$, respectively. For diatomic molecules the matrix elements can be calculated using recurrence relations for the spherical harmonics $Y_J^M(\theta,\phi)$ [30] and are included here for convenience:

$$\begin{aligned}\langle J'M'|e^{i2\phi}\sin^2\theta|JM\rangle &= \delta_{M',M+2}\left[H_{J-1}^{-M-1}H_{J-2}^{-M-2}\delta_{J',J-2} + H_J^M H_{J+1}^{M+1}\delta_{J',J+2}\right.\\ &\quad\left. - \left(H_{J-1}^{-M-1}H_{J-1}^{M+1} + H_J^{-M-2}H_J^M\right)\delta_{J',J}\right],\\ \langle J'M'|e^{-i2\phi}\sin^2\theta|JM\rangle &= \delta_{M',M-2}\left[H_{J-1}^{M-1}H_{J-2}^{M-2}\delta_{J',J-2} + H_J^{-M}H_{J+1}^{-M+1}\delta_{J',J+2}\right.\\ &\quad\left. - \left(H_J^{-M}H_J^{M-2} + H_{J-1}^{M-1}H_{J-1}^{-M+1}\right)\delta_{J',J}\right],\end{aligned}$$

where

$$H_J^M = \left[\frac{(J+M+1)(J+M+2)}{(2J+1)(2J+3)}\right]^{1/2}.$$

APPENDIX B: SOLUTION OF DYNAMICAL EQUATIONS

1. Pumping by impulsive dynamic Stark control

Given the relatively low fluence of the pump pulse, we can assume that there is negligible population transfer induced between the rotational levels; we also assume that the pump is unchanged during its propagation through the sample such that $A_1(z,\tau) = A_1(\tau)$ on the interval $-\infty < \tau < \tau_A$, and $A_1(\tau \geqslant \tau_A) = 0$. The Liouville equation for off-diagonal elements of the density matrix is then given by [31]

$$\frac{\partial\rho_{jk}}{\partial\tau} = i(i\Gamma_{kj} + \Omega_{kj})\rho_{jk} - \frac{iw_{jk}}{4\hbar}U_{jk}^{\mathrm{lin}}|A(\tau)|^2. \qquad \text{(B1)}$$

Stark shifting of diagonal terms in the density matrix has been ignored because it only results in an absolute phase shift. With zero initial coherence in the medium, Eq. (B1) can be integrated, with solution

$$\rho_{jk}(z,\tau) = -i\frac{w_{jk}}{4\hbar}U_{jk}^{\mathrm{lin}}\int_{-\infty}^{\tau}d\tau' \times[|A_1(\tau')|^2 e^{-\Gamma_{kj}(\tau-\tau')}e^{i\Omega_{kj}(\tau-\tau')}]. \qquad \text{(B2)}$$

2. Amplification by transient stimulated Raman scattering

In the limit of unsaturated Raman gain, with the amplification pulse $A_2(z,\tau) = A_2(\tau)$ on the interval $\tau \geqslant \tau_A$, and w_{jk} constant, the coupled equations for the Stokes sidebands and the coherences are [28]

$$\frac{\partial B_{jk}^{\mathrm{L}}}{\partial z} = i\beta_{kj}A_2(\tau)Q_{jk}(z,\tau), \qquad \text{(B3)}$$

$$\frac{\partial Q_{jk}}{\partial\tau} = -\Gamma_{kj}Q_{jk} - i\kappa_{jk}A_2^{*}(\tau)B_{jk}^{\mathrm{L}}(z,\tau), \qquad \text{(B4)}$$

where

$$Q_{jk}(z,\tau) = \rho_{jk} e^{-i\Omega_{kj}\tau}.$$

Assuming some initial coherence $Q_{jk}(\tau_A)$ is present in the medium before the arrival of the amplification field, and setting $B^{\mathrm{L}}_{jk}(0,\tau) = 0$, at times $\tau > \tau_A$ the solutions for the amplified coherences are

$$Q_{jk}(z,\tau) = Q_{jk}(\tau_A) e^{-\Gamma_{kj}(\tau-\tau_A)} I_0[\sqrt{4h_{jk}(\tau)z}], \quad \text{(B5)}$$

where $I_0(x)$ is the modified Bessel function of order 0. Writing out the full expression for the coherences using Eq. (11) as an initial condition yields Eq. (12).

3. Parametric scattering of probe pulse

The rotational coherence is measured by scattering an ultrashort probe pulse from the excited molecules. The input probe pulse $\boldsymbol{E}_3(0,\tau)$ is $\hat{\mathbf{x}}$ polarized, while the analyzing polarizer only transmits $\hat{\mathbf{y}}$-polarized light to the detector. The probe field is then given by

$$\boldsymbol{E}_3(z,\tau) = \tfrac{1}{2}\left\{\left[A^x_3(z,\tau)\hat{\mathbf{x}} + A^y_3(z,\tau)\hat{\mathbf{y}}\right] e^{-i\omega_3\tau} + \text{c.c.}\right\},$$

where $A^y_3(0,\tau) = 0$. It is assumed that the coherence induced by the pump and amplification pulses is unchanged by the propagation of the probe so Eq. (12) may be used to calculate the medium polarization.

In the slowly varying envelope approximation, the wave equation is

$$\frac{\partial \boldsymbol{A}_3}{\partial z} = i\frac{\omega_3}{2\epsilon_0 c}\boldsymbol{\mathcal{P}}(z,\tau), \quad \text{(B6)}$$

where the analytic function for the polarization density is given by

$$\boldsymbol{\mathcal{P}}(z,\tau) = N\langle\boldsymbol{\alpha}\rangle\cdot\boldsymbol{A}_3(z,\tau).$$

The components of Eq. (B6) reduce to the coupled equations

$$\begin{aligned}\frac{\partial A^x_3}{\partial z} &= i\frac{N\omega_3\Delta\alpha}{4\epsilon_0 c}\langle\sin 2\phi\sin^2\theta\rangle A^y_3(z,\tau),\\ \frac{\partial A^y_3}{\partial z} &= i\frac{N\omega_3\Delta\alpha}{4\epsilon_0 c}\langle\sin 2\phi\sin^2\theta\rangle A^x_3(z,\tau).\end{aligned} \quad \text{(B7)}$$

The initial condition for the probe is $\boldsymbol{A}_3(0,\tau) = A^x_3(0,\tau)\hat{\mathbf{x}}$; for sufficiently small coherences, the change in $A^x_3(z,\tau)$ will be negligible so we may set $A^x_3(z,\tau) = A^x_3(0,\tau)$. Equation (B7) may then be integrated with formal solution,

$$\begin{aligned}A^y_3(z,\tau) = \frac{N\omega_3\Delta\alpha}{8\epsilon_0 c}A^x_3(\tau)\sum_{jk}\int_0^z dz'\{&[\rho_{jk}(z',\tau)(\mathrm{e}^{i2\phi}\sin^2\theta)_{kj}\\ &-\rho_{jk}(z',\tau)(\mathrm{e}^{-i2\phi}\sin^2\theta)_{kj}]\}.\end{aligned} \quad \text{(B8)}$$

Using the selection rules for $e^{\pm i2\phi}\sin^2\theta$ (see Appendix A) yields Eq. (16).

[1] P. R. Brooks, Science **193**, 11 (1976).
[2] R. Velotta, N. Hay, M. B. Mason, M. Castillejo, and J. P. Marangos, Phys. Rev. Lett. **87**, 183901 (2001).
[3] P. Hockett, C. Z. Bisgaard, O. J. Clarkin, and A. Stolow, Nat. Phys. **7**, 612 (2011).
[4] P. Emma, R. Akre, J. Arthur, R. Bionta, C. Bostedt, J. Bozek, A. Brachmann, P. Bucksbaum, R. Coffee, F. Decker *et al.*, Nat. Photonics **4**, 641 (2010).
[5] M. Altarelli, R. Brinkmann, M. Chergui, W. Decking, B. Dobson, S. Düsterer, G. Grübel, W. Graeff, H. Graafsma, J. Hajdu *et al.*, DESY Report **97** (2006).
[6] H. Stapelfeldt and T. Seideman, Rev. Mod. Phys. **75**, 543 (2003).
[7] P. J. Bustard, G. Wu, R. Lausten, D. Townsend, I. A. Walmsley, A. Stolow, and B. J. Sussman, Faraday Discuss. **153**, 321 (2011).
[8] B. J. Sussman, Am. J. Phys. **79**, 477 (2011).
[9] J. Reuss, *Atomic and Molecular Beam Methods* (Oxford University Press, Oxford, 1988), Chap. 11, pp. 276–292.
[10] B. Friedrich and D. Herschbach, Nature (London) **353**, 412 (1991).
[11] H. J. Loesch and A. Remscheid, J. Chem. Phys. **93**, 4779 (1990).
[12] B. Friedrich and D. Herschbach, J. Phys. Chem. A **103**, 10280 (1999).
[13] H. Sakai, S. Minemoto, H. Nanjo, H. Tanji, and T. Suzuki, Phys. Rev. Lett. **90**, 083001 (2003).
[14] U. Buck and M. Fàrnìk, Int. Rev. Phys. Chem. **25**, 583 (2006).
[15] P. J. Bustard, B. J. Sussman, and I. A. Walmsley, Phys. Rev. Lett. **104**, 193902 (2010).
[16] A. Penzkofer, A. Laubereau, and W. Kaiser, Prog. Quantum Electron. **6**, 55 (1979).
[17] R. Baumgartner and R. Byer, IEEE J. Quantum Electron. **15**, 432 (1979).
[18] Y. Yan, E. Gamble, Jr., and K. Nelson, J. Chem. Phys. **83**, 5391 (1985).
[19] J. P. Heritage, T. K. Gustafson, and C. H. Lin, Phys. Rev. Lett. **34**, 1299 (1975).
[20] M. Morgen, W. Price, L. Hunziker, P. Ludowise, M. Blackwell, and Y. Chen, Chem. Phys. Lett. **209**, 1 (1993).
[21] G. Herzberg, *Molecular Spectra and Molecular Structure: 1. Spectra of Diatomic Molecules* (Van Nostrand, Princeton, 1950).
[22] G. C. Herring, M. J. Dyer, and W. K. Bischel, Phys. Rev. A **34**, 1944 (1986).
[23] B. J. Sussman, J. G. Underwood, R. Lausten, M. Y. Ivanov, and A. Stolow, Phys. Rev. A **73**, 053403 (2006).
[24] B. Friedrich and D. Herschbach, Phys. Rev. Lett. **74**, 4623 (1995).
[25] R. W. Boyd, *Nonlinear Optics* (Academic Press, New York, 1992).
[26] R. W. Minck, E. E. Hagenlocker, and W. G. Rado, Phys. Rev. Lett. **17**, 229 (1966).
[27] R. Holmes and A. Flusberg, Phys. Rev. A **37**, 1588 (1988).
[28] M. G. Raymer and J. Mostowski, Phys. Rev. A **24**, 1980 (1981).
[29] F. LeKien, J. Q. Liang, M. Katsuragawa, K. Ohtsuki, K. Hakuta, and A. V. Sokolov, Phys. Rev. A **60**, 1562 (1999).
[30] G. B. Arfken and H. J. Weber, *Mathematical Methods for Physicists*, 6th ed. (Academic Press, New York, 2005).
[31] V. P. Kalosha and J. Herrmann, Phys. Rev. Lett. **85**, 1226 (2000).